Nano Research
ISSN 1998-0124 CN 1
https://doi.org/10.1007/
Review Article

Recent advances in tip-enhance[d] … designs

Da Xu[1], Boqun Liang[2], Yang Xu[2], and Ming Liu[1,2] (✉)

[1] Department of Electrical and Computer Engineering, University of California, Riverside, CA 92521, USA
[2] Materials Science and Engineering, University of California, Riverside, CA 92521, USA

© Tsinghua University Press 2022

Received: 27 August 2022 / Revised: 18 October 2022 / Accepted: 19 October 2022

ABSTRACT

Tip-enhanced Raman spectroscopy (TERS) imaging is a super-resol[ution] … surface-enhanced Raman spectroscopy (SERS) and scanning probe mi[croscopy] … from the former and the nanoscale spatial resolution from the … spectroscopic characterization technique for chemical analysis, … critical factor determining the TERS imaging quality, are expect[ed] … minimized scattering background for the generation of Raman si[gnal] … development, numerous probe design concepts have been proposed a[nd] … overview of the state-of-the-art TERS probe designs, from the wo[rking] … reviewing the recent development of TERS configurations and the … platforms, optical excitation/collection techniques, and probe p[reparation] … probe designs, including the remote-excitation probes, the wa[veguide] … nanofocusing probes, the nanowire-assisted selective-coupling p[robes] … discussion focuses on a few critical aspects, including the su[rface] … conversion efficiency, working frequency, and controllability. … perspective on the future of TERS.

KEYWORDS

tip-enhanced Raman spectroscopy, plasmonics, scanning probe … nanofocusing

1 Introduction

Raman spectroscopy provides fingerprint information to iden[tify] different chemical bonds and has become a powerful techniqu[e] for chemical analysis [1, 2], biosensing [3, 4], etc. In a Raman measurement, the sample illuminated by a la[ser] beam scatters light with different frequencies from the exc[itation] through inelastic scattering processes that involve the en[ergy] exchange between the incident photons and the local atomic vibrations. However, compared with the elastic Rayleigh scat[tering] process, the inelastic Raman scattering is extremely weak (a[bout] 10^{-6} of the incident intensity) and consequently becomes a challenging mission for signal detection. Fortunately, t[he] development of plasmonics in the past decades has tremendous[ly] increased the sensitivity of Raman spectroscopy by employing electric field enhancement induced by surface plasmon resona[nce] (SPR).

SPR describes the collective electron oscillations arising … the interaction between the incident light and the free elec[trons] … a metal, whose inertia, in combination with the electric … forces, gives rise to the accumulation of … a nanoscale volume. This highly … commonly called "hot spots", they exist …

metal surfaces with large curvat[ure] … nanoparticle aggregates. Such loca[lized] field enhancement [5] … the surface-enhanc[ed Raman] scattering (SERS), initially rep[orted] [6] … 1974 [7] and explained by … Jeanmaire … 1977, uses the localized surface plasm[on] … of an amorphous metal film to … cross-sections of the specimen. … development, SERS has pushed the … the single-molecule level [9–11] and has been appli[ed] … range of applications [12], such as chemical reaction mechanism stud[y] [13]. Despite the continuous improvem[ent] … correlating the chemical informa[tion] … remains elusive, particularly in … other optical microscopies, the … restricted by the optical diffr[action] … excitation wavelength [14], larger than the … visible wavelength range. More… [illegible] … distributions of SERS substrates [15] … chemical … inhomogeneity. Overcoming the …

Address correspondence to [illegible] .com

nanoscale or even few-nanometer [illegible] creating high-intensity nano[illegible] position control, which can [illegible] SERS measurement with scann[illegible] combine the incredible chemi[illegible] excellent spati[illegible] of tip-enhanced Raman spect[roscopy (TERS)] [illegible] proposed by Wessel in 1985 [16] and [illegible] demonstrated by Stöckle, Hayazawa, Anderson, and Pettinger [illegible] 2000, individually [17–20]. Since then, tremendous efforts have been made to improve the [illegible] resolution with several SPM [illegible] [21–23]. Among these mechanisms, scanning tunneling microscopy (STM) and atomic force microscopy (AFM) are preferred, since the former can image the morphology with atomic resolution, while the latter can be accommodated with commercial AFM probe manufacturing [24].

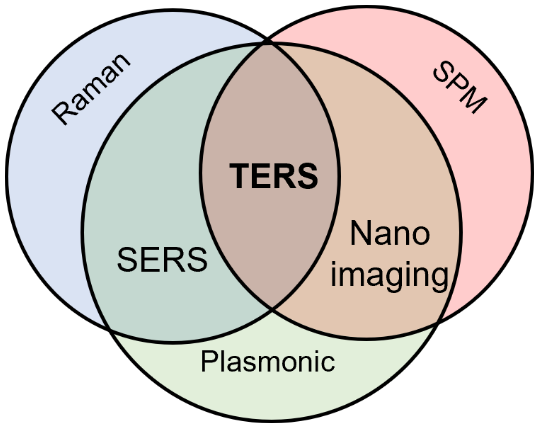

Figure 1 Venn diagram showing the relation among plasmonic, SPM, and Raman spectroscopy.

The most critical step in TERS imaging is converting the incident light into the plasmonic resonance at a probe tip f[illegible] field illumination. The conversion efficiency of a probe det[illegible] the success of TERS imaging, not only because a high-inten[illegible] hotspot is essential for Raman signal generation [25], but [illegible] because of the restriction on incident power to avoid th[illegible] background Raman scattering. Most TERS probes utilize the lightning-rod effect and LSPR to generate hotspots. The lightning-rod effect stems from the electric field enhancement at the proximity of a sharply curved metal surface, such as edges, corners, or sharp metallic tips, which concentrate the [illegible] electrons in a metal driven by the electric field of the in[illegible] to a tightly [illegible] [26, 27]. [illegible] lightning-rod effect usually [illegible] fabrication methods, such as deposition of metal films on commercial AFM probes, and can work at a broad wavelength range, from ultraviolet (UV) [illegible] [28, 29]. [illegible] rod can also be a metallic nanoparticle that serves as a nanoantenna with a large scattering cross-section and improved conversion efficiency [30, 31]. The flexibility of nanoantenna designs allows novel functionalities, such as measuring the magnetic field [32, 33]. Moreover, [illegible] its working frequency can be [illegible] The LSPR is the coherent [illegible] electromagnetic waves and confined [illegible] wavelength of the LSPR can be tuned by the tip shape [illegible] maximize the charge concentration on the tip apex [illegible] be achieved by attaching [illegible] [34], [illegible] nanocones [35], aluminum [illegible] [36], [illegible] nano[illegible] [37], or apex-adjusted [illegible] [38, 39] [illegible]

[illegible] LSPR [illegible] sharpened [illegible] [40] [illegible] Depending on the [illegible] 5 nm [illegible] [41] [illegible] 10 [illegible] larger than th[illegible] area [illegible] (TERS) imaging [illegible] experimentally [43, 44] [illegible] enhanced signals. Although this [illegible] suppressed by [illegible] through a separated scanning wit[illegible] noise is still remarkable due to [illegible] Raman signals.

Recently, numerous research [illegible] removing the surface-plasmon-pol[illegible] from the probe tip to reduce the [illegible] field noise. However, since the [illegible] moderate [illegible] (~10 [illegible]) that is much [illegible] than that of a [illegible] adiabatic nanofocusing process i[illegible] for the considerable [illegible] [45–50]. [illegible] has motivated the development of [illegible] grating couplers [51, 52], [illegible] conical plasmonic [illegible] [48, 53] [illegible] couplers [54, 55], and tapered metal-insu[illegible] waveguides [56].

In this review, we will first [illegible] TERS and discuss the novel tip [illegible] nanofocusing methods. After tha[illegible] applications and prospects, whi[illegible] future TERS designs.

2 Working principle

2.1 SPM techniques for TERS

TERS is the integration of SPM a[illegible] non-trivial [illegible] for ambient ope[illegible] the creation of a high-quality [illegible] [illegible] SPM configurations could provide [illegible] [illegible]

2.2 Optical signal collection

Currently, most TERS setups are built upon a scattering-type
field scanning optical microscopy (NSOM), which includes a
excitation laser, an optical microscope system, a piezo-sta
maintain the tip-sample distance, and an optical spectrome
spectroscopic analysis. A high-numerical-aperture (NA) objec
lens is usually needed to minimize the size of the focused
which is, however, problematic for the probe alignment and
with the mechanical stability of the system to maintain the
alignment with a sub-50 nm accuracy.

Based on the illumination and signal collection methods,
various types of TERS designs can be categorized into three
groups: the bottom illumination mode [59–61], side illumination mode [
illumination mode, Fig. 2(c)). Due to
space constraints in an instrument, the illumination and s
collection usually share the same objective lens, which is
an oil lens or a parabolic mirror with a high NA (0.9–1.4)
bottom illumination configuration [62, 63], or a long-working-
distance lens with a moderate NA (0.3–0.7) for the side
illumination. In the bottom illumination mode, a radially
polarized laser beam is preferred [64, 65], since it
has the cylindrically converging wave interference around the
optical axis and forms the predominant polarization component
along with the longitudinal direction [66], which can effectively
excite the longitudinal plasmonic oscillation in the tip. The
calibration of the radial polarization can be realized by p
thin Ag film on the sample stage and examining the focal s
pattern of the reflected light. Since a radially polarized a
polarized to the metal surface, it efficiently excites SPPs
directions, leading to the emission of a component with certa
momentums in the reflected light and consequently forming
dark ring at the center [67].

Compared with the bottom illumination configuration, the si
illumination configuration can break the restrictions on sa
transparency and thickness. It puts fewer requirements on
beam polarization, as a p-polarized [illegible]
efficiently excite the gap plasmons between the tip and the
substrate. However, since the [illegible]

use a medium-NA objective lens t
aligning its acceptance angle w
radiation lobes of a TERS probe
efficiency [68–70]. This setting i
the surface roughness including
with vestiges of crystal facets
screening probes by examining th
and only keeping the on-resonanc
Top illumination can obtain bot
side illumination configurations
can be used for [71], tight [illegible] focus mechanism
samples is not required. However
incident and scattered light, th
specially designed, which adds d
vacuum and low-temperature syste
In recent years, Fig. 2(c)(iv) [illegible] become
proven as a promising method for
unique feature of nanofocusing
launching region from the TERS
reduce the negative impact of th
Another critical factor determi
radiation channel of an electric
TERS tip. Theoretical analyses h
radiation rate from the dipole
decay rate (5.4% and 19%, for th
metal substrate [72], respectively)
dissipation is in the form of a
metal probe surface (63% on a
metal substrate). Likewise, the
extract the Raman signals from a
significant non-radiative dissip
enormous density [73] SPP states been
accessed in TERS measurements.

2.3 TERS probe preparation te

An STM-based TERS usually employ
metal probes. Conventionally, the STM probe
[illegible] [74] [illegible]

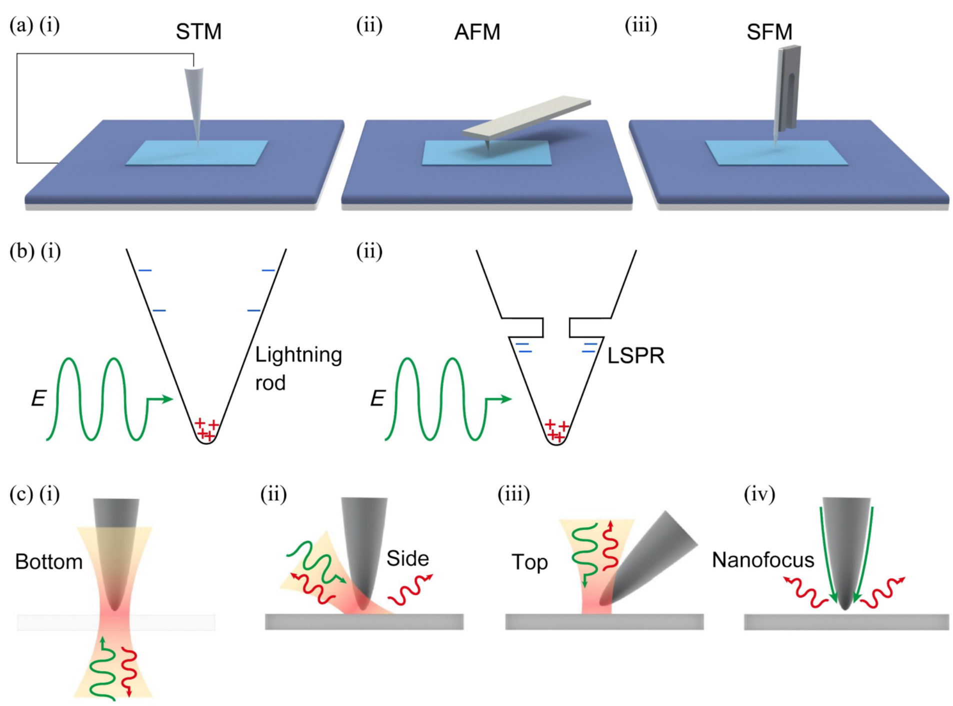

Figure 2 Schematics of TERS configurations. (a) Different SPM configurations [illegible] popular field-enhancement mechanisms adopted in TERS: (i) lightning ro[illegible] illumination, (iii) top illumination, and (iv) nanofocusing.

to form dangling bonds for atoms [58]. However, these metals are not suitable for SERS due to their large plasmonic loss in the visible range [75]. Instead, noble metals are more frequently used. The popular fabrication method to prepare an STM-TERS probe is electrochemical etching of an Ag or Au thin wire [76], as shown in Fig. 3(a). The plasmonic loss can be further reduced by crystallizing the wire by annealing [77]. The enhancement of an etched probe is sensitive to both the metal conductivity and the tip morphology, which requires the careful control of the etching parameters [78, 79], including the precise control with current cut-offs and optical feedbacks to prevent over-etching [80]. Electrochemical etching procedures are mature in preparing tips with a tip radius curvature around 20 nm [79]. A sharper probe can be prepared by assembling a chemically synthesized tapered silver nanowire (AgNW) on a metallic probe [81], in which the AgNW tip radius can be reduced to ~5 nm.

AFM-TERS probes are usually prepared by depositing a thin Ag or Au film on a silicon cantilever (Fig. 3(c)) [82, 83]. Various film thicknesses (10–70 nm) and roughness values (from the smooth to the rough) have been reported [84–86] in the literature. The film qualities can be controlled by thermal evaporation parameters, including the deposition rate, substrate temperature, chamber pressure and source/probe positions. In general, studies show that a low deposition rate [illegible] nm/s) tends to give a smooth surface, while the chamber vacuum has a more negligible effect on surface roughness and the size of the grain island is more related to the film thickness. However, further studies on the influence of ultra-low deposition rate [illegible] to 0.14 nm/s) showed that the film roughness increases again with the decrease in deposition rate due to the thermal migration of high-energy metal atoms [87]. The thermal migration and aggregation of metal atoms form large grains [illegible] 85 nm) on the film, which makes the AFM-TERS probe blunt. Figure 3(d) demonstrates a template-stripping fabrication technique that can restrain the atom migration through the confinement of a sharp-curvature template, mass producing high-quality, uniform, and [illegible] probes [88, 89].

Assembling metal nanoparticles on the apex of an AFM probe is another commonly used preparation method [illegible]

[illegible] probes. Chemically [illegible] Au [illegible] measurement [illegible] through a [illegible] method [90], a [illegible] is attached [illegible] focused [illegible] Au [illegible] deposition [illegible] (Fig. 3(f)) [92]. [illegible] antenna [illegible] picking up [illegible] (e.g., Ag or Au [illegible] 80–400 nm [illegible]) [illegible] Compared to the TERS tips with [illegible] apex, the intrinsic quantum eff[illegible] antennas can achieve both more [illegible] enhancement [illegible] ratio is also [illegible] reported an assembling method [illegible] Ag nanocubes (AgNCs) on blunt [illegible] Langmuir–Blodgett [93] (Fig. 3(h)) [illegible] sub-50 nm resolution was reported [illegible] consist[illegible] used large [illegible] [94]. Moreover, AgNCs at [illegible] can form plasmonic cavities w[illegible] approaching [illegible] making it appealing f[illegible] detections. Besides these conven[illegible] probe concepts have attracted br[illegible] which will be discussed in the n[illegible]

3 Emerging TERS probe [illegible]

The development of TERS probes [illegible] implementation of plasmonic nano[illegible] antennas [illegible], c-shaped [98, 99] [illegible] gratings [100, 101, 102] [illegible] to increase [illegible] conversion efficiency and the [illegible] scattering cross-section of a [illegible] fraction [103] of the [illegible] factor are not satisfactory. [illegible] focused on nanofocusing mechanis[illegible] SPP excitation region and the [illegible] reduce the impact of large [illegible] probes with [illegible] corresponding nanofocusing mecha[illegible]

3.1 Nanofocusing probes

The nanofocusing [illegible] (< 10 nm) [illegible] 1997, Nerkararyan [illegible] that SPP waves [illegible] metal [illegible] the apex of a [illegible] [50] [illegible] Later, [illegible] this [illegible] TERS [illegible]

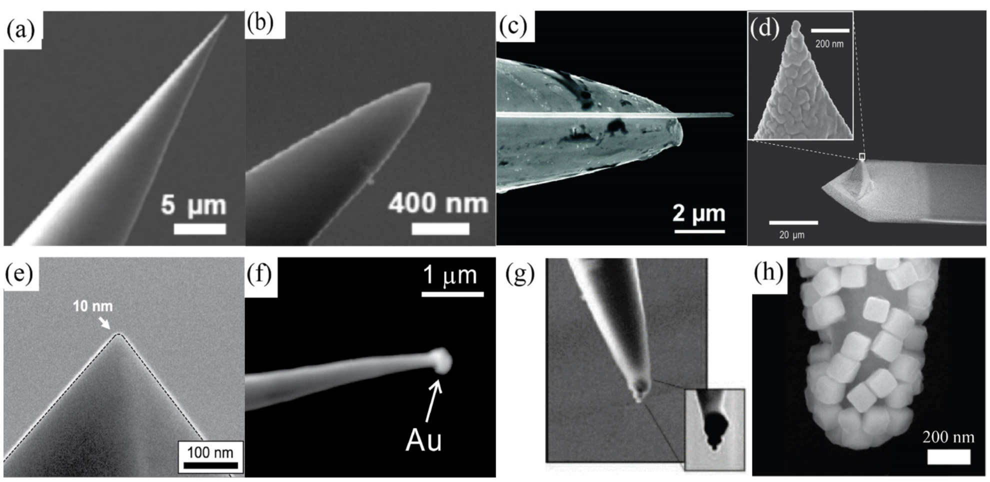

Figure 3 SEM images of conventional TERS probes are prepared through differe[illegible] etching of Au wires. (a) and (b) [76] © American Institute of Physics 2009. [illegible] tungsten probe. Reproduced with permission from Ref. [81], © The Royal Society of Chemistry 2019. (d) Th[illegible] permission from Ref. [83], © American Chemical Society 2014. (e) The Au [illegible] Ref. [88], © American Chemical Society 2012. (f) [illegible] tips made by assembling nanoparticles [illegible] [92] [illegible] © [illegible] permission from Ref. [90], © American Physical Society 2012. (h) Reproduced with permission [illegible] © American Chemical Society [illegible]

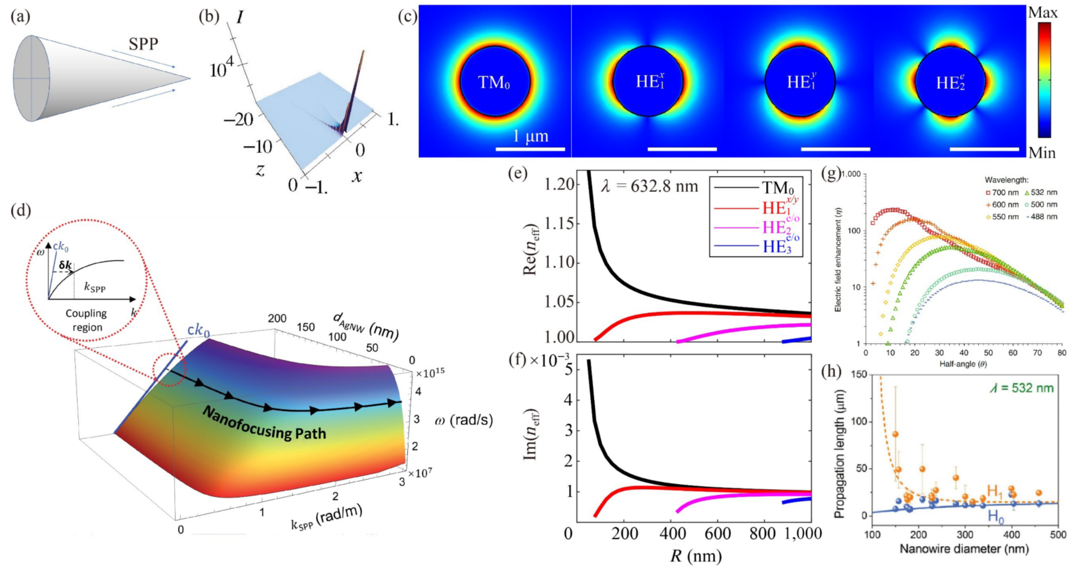

Figure 4 Plasmonic nanofocusing. (a) Schematic of the nanofocusing process on [illegible] tip apex. Reproduced with permission from Ref. [48], © American Physical Society 2011. (c) The elect[illegible] waveguide. (d) The 3D dispersion relation of the SPP TM$_{01}$ mode at different frequencies and diff[illegible] nanofocusing path along a tapered waveguide and the inset shows the mom[illegible] of the effective indices of different modes with different waveguide diameters. Only TM$_0$ can be super[illegible] enhancement after nanofocusing at the tip apex. Reproduced with permission from Ref. [107], © Springer Science [illegible] LLC 2006. (h) The experiment results of measured propagation length [116], © Tsinghua University [illegible] Springer-Verlag Berlin Heidelberg 2017.

conical structure in 2004 [104]. Stockman studied the adiabatic deceleration and asymptotic ... of SPP on a tapered metal waveguide and predicted that three orders of magnitude enhancement in intensity could be achieved by superfocusing [48] (Fig. 4(b)), which ignited the nanofocusing ... A cylindrical metal waveguide can support multiple SPP modes on its surface, including a fundamental mode TM$_0$ and high order modes, e.g., HE$_1$ [105]. Among these modes, only the TM$_0$ mode has no cut-off radius and can keep tightly bound to the metal surface while propagating towards the tip apex (Figs. 4(e) and 4(f)). Figure 4(d) depicts the 3D dispersion relation of the SPP at different nanowire diameters. Black arrows indicate the adiabatic increase in SPP wavenumber k_{SPP} with the decrease of the waveguide diameter, exhibiting the route of SPP in the nanofocusing. The large k_{SPP} at the end of the nanofocusing process leads to a superfocused plasmonic mode localized at the tip apex, which can be used for nano-imaging.

The adiabatic nanofocusing requires the eikonal approximation restricting the probe slope to less than 0.1. However, a slim probe also means a long propagation distance, which significantly attenuates the SPP intensity due to the short propagation length of the TM$_0$ mode even in a [illegible] [106]. Simulation [illegible] revealed that the optimized taper half angle ... under the 488 nm excitation (Fig. 4(g)) [107, 108]. The low plasmonic propagation loss under a long excitation wavelength can support a long propagation length and thus a tiny taper angle.

Another determining factor in superfocusing is surface roughness. Norris et al. have demonstrated that the propagation length of a planar SPP on an ultrasmooth metal film is several times longer than that on conventional films, primarily benefiting from the small surface roughness (0.34 nm) compared with that of a conventional film prepared through thermal evaporation (2.18 nm) [109]. So far, there is no experiment to study the influence of surface roughness on the superfocusing process, but its impact is expected to be prominent, as the SPP with the ... vulnerable to the roughness ...

... propagation ... TM$_0$ ... single ... SPP ... (Fig. 4(h)) [113] ... three orders of ... propagation length than ... few micrometers, which needs to ... the nanofocusing probe design.

The efficient excitation of SPP requires the momentum matching between the ... mode or the momentum mismatch ... prism [110], a single or multiple ... [37, 111], a plasmonic ... [112], which are discussed in detail in ... section.

3.2 Remote excitation of SPP in the nanofocusing probe

Inspired by the Kretschmann configuration ... localized at the tip apex, which ... used in SPP applications, the ea[illegible] couplers into the TERS probe wa[illegible] micrometer-sized glass prism on t[illegible] ... combination of milling and focu[illegible] deposition of tetraethyl orthosi[illegible] 2001 [20]. Although the design idea ... its near-field optical imaging p[illegible] stringent SPP excitation conditi[illegible] such as the incident angle and ... challenging for the proposed con[illegible] was re-visited by Zhang et al., ... cantilever AFM probe into a pris[illegible] TERS measurements [114].

In 2007, Ropers et al. introduc[illegible] gold tip shaft [111] ... employed in various nonlinear op[illegible] [115] (Fig. 5(a)). Although the grating co[illegible] mature in integrated photonic c[illegible] coupling efficiency is ... [116] ... conical probes is expected ... the probe shaft ... 10% ... under ... [115] ...

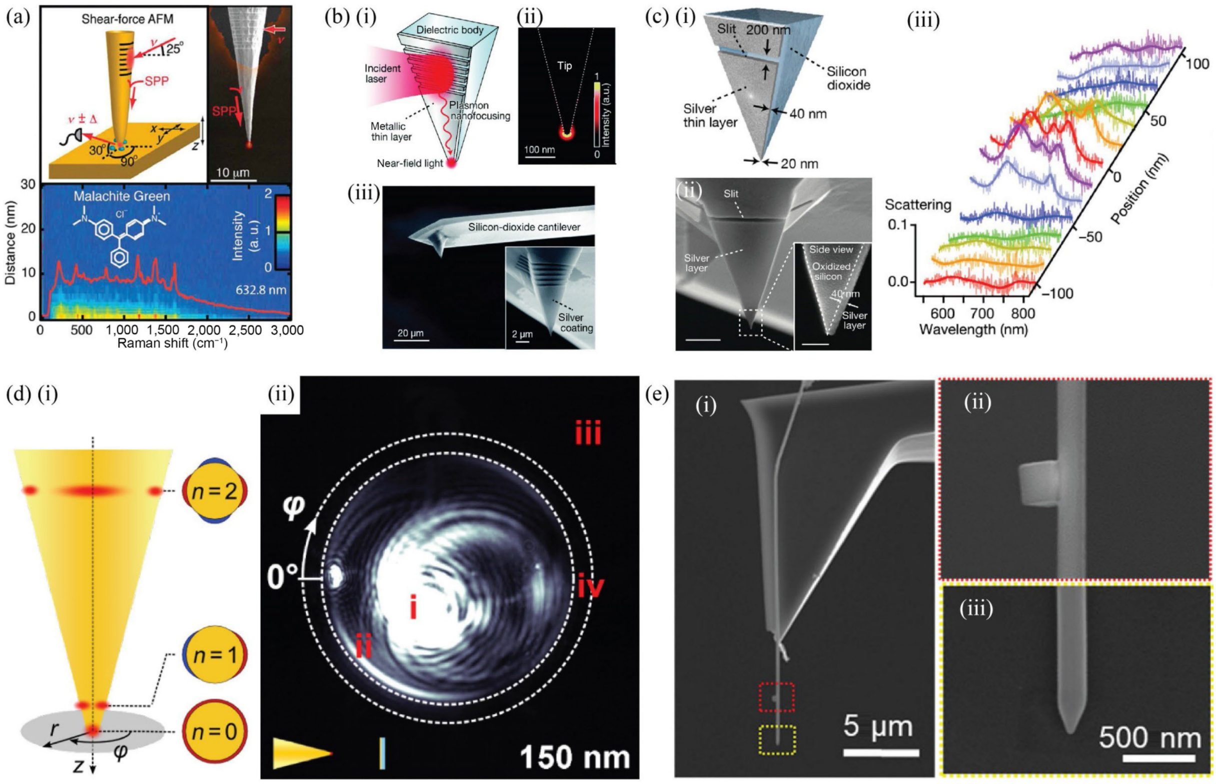

Figure 5 Remote excitation probes. (a) Top: a gold probe with gratings on t… under different tip-to-sample d… [115], © American Chemical Society 2010. (b) … remote gratings: (i) schematic of the probe, (ii) simulation … [117], © The Royal Society of Chemistry 2016. (c) Ag-coated AFM contact probe wi… schematics and SEM images of the probe, and (iii) Raman … [118], © … T. et al. 2020. (d) Schematics of the SPP cut-off radii … [119], © … al. 2013. (e) AgNW-based TERS probe with a remote AgNC coupler: (i) the … in (i). Reproduced with permission from Ref. [122], © American Chemical Society 2018.

et al. designed and fabricated … AFM probe [117] (Figs. 5(b)(i)–5(b)(iii)) … technique close to mass production. … and experiment (Fig. 5(b)) results … can be coupled to the SPP … sufficient to measure the … carbon nanotubes (SWNT) [118] … (Fig. 5(c)).

The weight of the TM$_0$ mode excitation … coupler is critical to the … coupler is usually engraved … 30 to 50 μm away from the … range planar SPPs, which … HE$_{\pm1}$ modes, and other higher-order … only the TM$_0$ mode can be nanofocused … encountering … (Fig. 5(d)(i)). However … mode overlapping between … the tightly bound TM$_0$ … further reduced by its … measurements (Figs. 5(d)(ii)) … intensity of the TM$_0$ mode … [119]. … high-order modes become unbound … their cut-off radius, leading … propagate in the vicinity of … illuminates the sample as well … low spatial resolution. The … efficiency of the TM$_0$ mode … essential for high-performance TERS probes.

In this probe configuration … could be achieved by replacing the grating …

… a plasmonic coupler … propagation distance. … demonstrat… Accordingly … (Fig. 5(e)) … a single AgNC … scattering [120] … [121] … [2018] … through the self-assembly and … AgNC was placed … away from the … AgNW. … a … TM$_0$ … 4% of … [122] … nanowire …

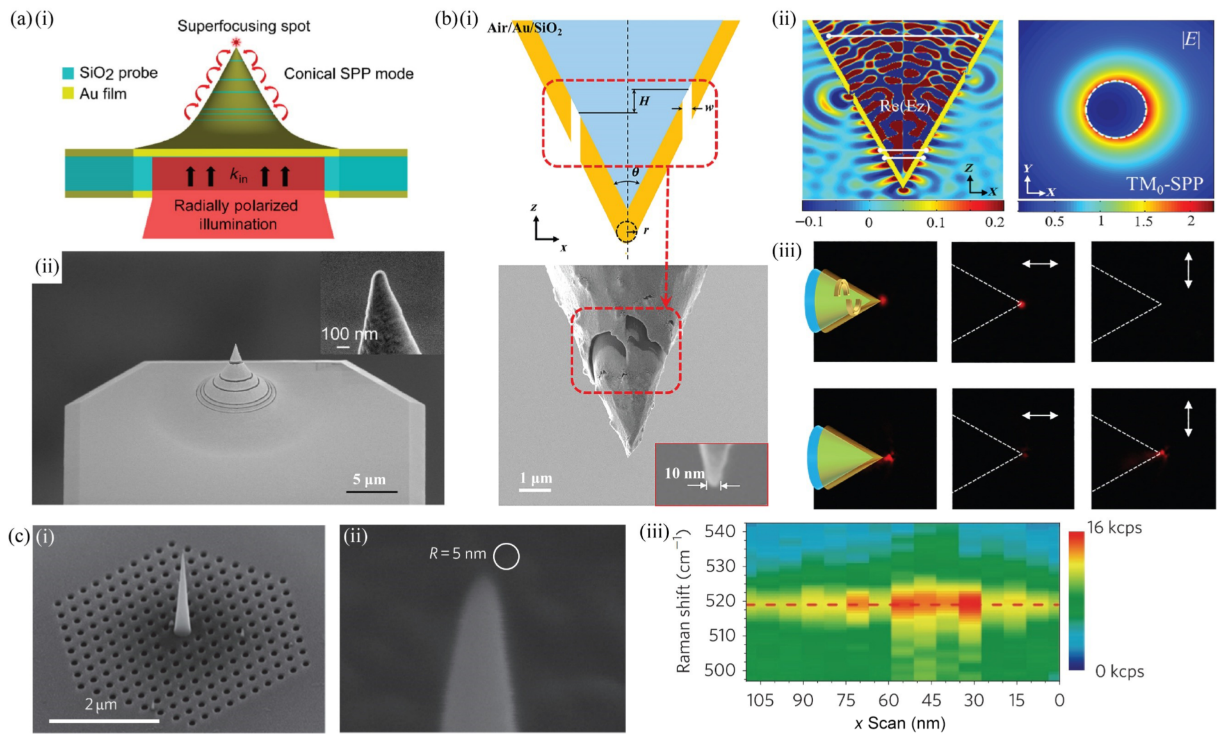

Figure 6 Remote excitation probes with special couplers. (a) The Au-coated c[illegible] into TM0 mode SPP. Reproduced with permission from Ref. [123], © American Chemical Society 2017. (b) The [illegible] semicircular slits to couple [illegible] mode SPP. (i) Schematic [illegible] fiber-[illegible] SEM image of [illegible] tip, and (iii) polarization-dependent excitation. Reproduced with permission from Ref. [124], © [illegible] 2021 [illegible] (ii) SEM images of the probe [illegible] Raman [illegible] Reproduced with permission from Ref. [52], © [illegible]

result, a throughput of 3.28% and [illegible] signal-to-noise ratio (SNR) of [illegible] simplified the polarization requirement [illegible] designing a plasmonic probe with [illegible] slits that can excite the TM0 mode SPP [illegible] polarized excitation [124] (Fig. 6(b)). The numerical [illegible] further prove that the TM0 mode [illegible] checking its polarization. Although [illegible] limited to about 0.2%, the [illegible] the TM0 mode in the excited SPP [illegible] increased. The principle of SPP remote [illegible] excitation can also be realized with [illegible] crystal (PC) cavity. In Fig. 6(c), [illegible] cavity on an AFM cantilever [13] [illegible] the PC cavity through the FIB [illegible] the TM0 mode in the metal tip, which [illegible] of a silicon grating sample [illegible]

[illegible] have been demonstrated [illegible] requirement of high-efficiency coupling [illegible] SPP mode [illegible] efficiently excited by the li[illegible] [illegible] coupler. [illegible] mode [illegible] Ag NWs [illegible] metal-[illegible] Numerical simulations [illegible] Fig. 7(a) [illegible] Raman signal [illegible] piece of gold nanowire embedded [illegible] structure [138] (Fig. 7(b)). Since the coupli[illegible] between two parallel waveguides [illegible] region maximized its coupling ef[illegible]

3.3 Waveguide-based nanofocusing probes

Researchers have developed various nanofocusing [illegible] on an optical fiber platform [illegible] procedures. This section reviews the working [illegible] designs used in converting [illegible] to the superfocused SPP [125, 126] [illegible] and waveguide [127]. The key parameters [illegible] the excitation efficiency will also be discussed, including profile matching, phase constant matching, and adequate coupling lengths.

The excellent plasmonic properties of [illegible] nanowires, either prepared [illegible] (AAO-) template [128, 129] or the [illegible] mediated synthesis [130], have excited [illegible] interests in both the plasmonic [illegible] demonstrations of SPP excitation [131] [illegible]

3.4 Metal-coated nanofocusing [illegible]

Researchers have looked for alt[illegible] fabricated [illegible] aluminum oxide [illegible] describes the [illegible] After [illegible] [rep[illegible]

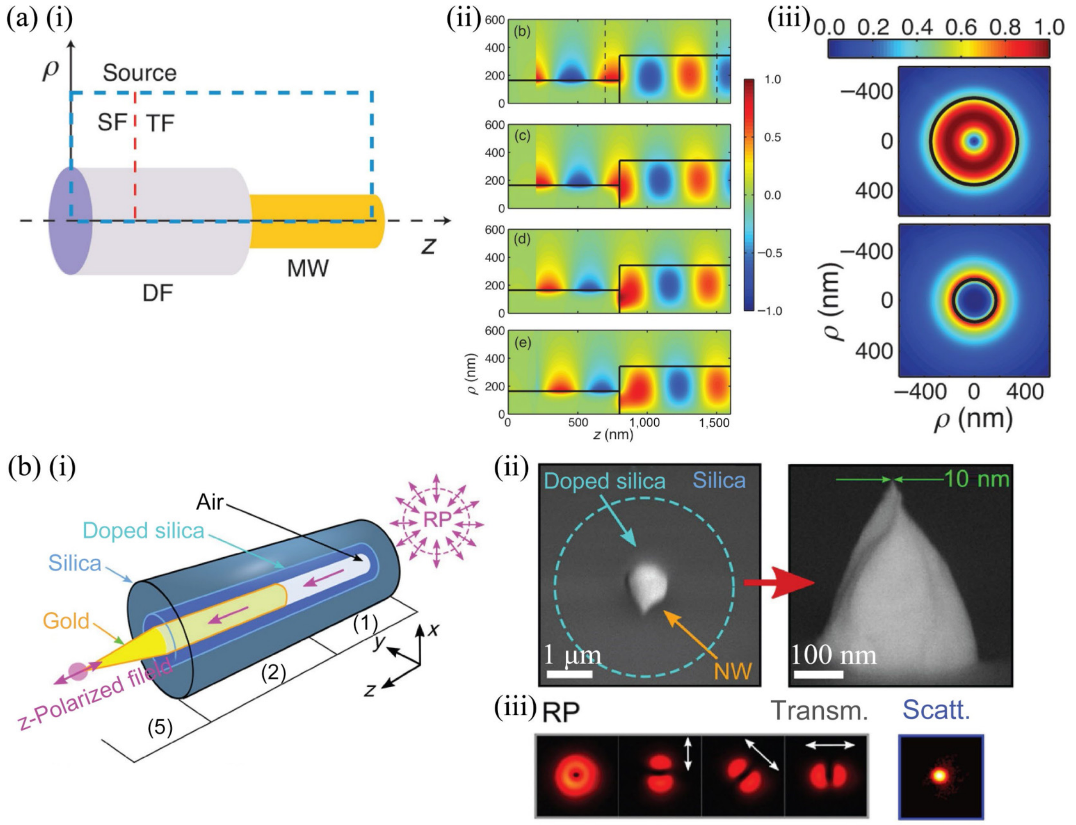

Figure 7 Waveguide-based nanofocusing probes. (a) The coupling from a dielec... simulation geometry. The dashed line between the scattered field (SF) ... distributions at different times of the fiber mode and (SPP) mode ... Reproduced with permission from Ref. [..], © American Chemical Society 2009. (b) A hybrid TERS probe with a gold nanowire in the core of a ste... verified the TM_0 mode of the SPP at the tip apex. Reproduced with permission from Ref. [..], © American Chemical Society 2016.

by the propagation constant ... direction [140], such as a tapered fiber probe ... SPP mode represents the time ... state.

In 2003, Bouhelier et al. ... nanofocusing of radially polarized near-field waves ... metal-coated tapered waveguide ... hotspot could be achieved at the tip apex through the constructive interference [141]. Janunts et al. introduced the LZ model to explain the SPP excitation process ... the coupling conditions to improve the transition efficiency between two lossless waveguides [55]. The coupling efficiency of amplitude transition between two waveguides (a and b) is determined by Eq. (1)

$$= -\exp(- \, / \,)$$

where $\left|\frac{d(\ )}{d}\right|$ describes the coupling strength and the difference between the propagation constants (β_a and β_b). In general, a high coupling efficiency requires a large modal overlap and a slow changing rate. The former can be realized by reducing ... increase the modal overlapping ... and the SPP mode at the outer surface ... can be achieved by reducing ... slow down the mode variation ... increase in SPP propagation length ... resulting in a trade-off in the probe design. By considering ... coupling between the fiber mode and the outer-surface SPP modes, Tugchin et al. reported ... efficiency and ~76% of a ...

considering a ... upper bound to the coupling eff... suggested that ... configuration ... SPP modes ... 10% [143] ... tip apex through the const... Although the numerical simula... experimental demonstration ... rather difficult ... 2015 by Tugchin et al., who coat... optical fiber with a thin film ... light to excite the SPP TM_0 mode ... Although a near-unity coupling ... achieved between a pure fiber mode ... experimental measurement could ... 0.3% [42]. This significant differen... experiment may originate from th... changing rates of propagation ... input in the theory, which can... Another problem with this config... around 100 nm due to the atom... deposition. To simplify the req... mode between the optical fiber ... method for asymmetric ... the TM_0 SPP ... enhanced ... TERS measurements ...

3.5 Nanowire-assisted selecti...

Tapered fiber ... technique ...

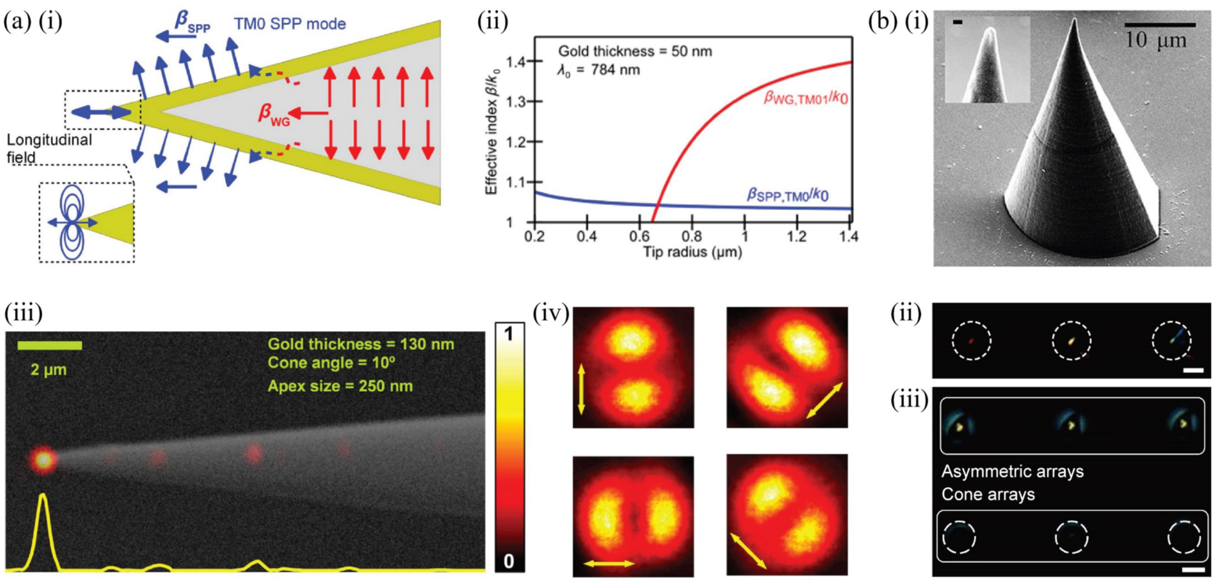

Figure 8 Metal-coated nanofocusing probes. (a) A gold-coated [illegible] mode: (i) [illegible] schematics of the probe, (ii) effective indices at different tip radii [illegible] examination at the fiber output [illegible] [142], © [illegible] 2015. [illegible] film [illegible] mode excitation: (i) the SEM image of an asymmetric probe. Scale b[illegible] red to green by angled incidences, (iii) tip brightness comparison betw[illegible] with permission from [141], © American Chemical Society 2018.

nanowire. For instance, Yan [illegible] at the single-cell level using [illegible] to a tapered optical [134] [illegible] 2019 [illegible] for the analysis [illegible] expanded the LZ transition model from two modes to multiple modes to explain the coupling between a tapered optical fibe[illegible] a plasmonic AgNW. They [illegible] could be selectively excited [illegible] [54]. As shown in Fig. 9(a)(i) [illegible] placed on the sidewall of the [illegible] LP_{01} mode in the fiber and the [illegible] TM_0 mode are not aligned, wh[illegible] overlapping coefficient and [illegible] coupling. As the light propa[illegible] the effective mode index gra[illegible] the mode index of the TM_0 [illegible] to its efficient excitation. [illegible] efficiency in zone 2 prevents [illegible] mode to the $TM_{\pm 1}$ mode through the [illegible] adiabatic passage [145]. [illegible] that around 70% of the incident [illegible] the TM_0 mode, as confirmed by Fig. [illegible] 9(a)(iv), which was later improved [illegible] taper profile through [146]. [illegible] benefitting from the atomica[illegible] uniform AgNW diameter, it [illegible] during the LZ transition. [illegible] demonstration of high coupli[illegible] coupling from the AgNW wave[illegible] efficient, which incubates t[illegible] STM-based NSOM TERS with [illegible] 9(a)(v)). By utilizing the ultra[illegible] the near-zero background il[illegible] demonstrated the absorption [illegible] imaging (Fig. 9(b)) and performed the [illegible] mapping of the longitudinal [illegible] SW-CNTs with 6 nm spatial r[illegible] infrared wavelength [147]. Benefitting from [illegible] electric field component at the [illegible] CNTs were for the first time [illegible]

3.6 Tapered MIM probes

[illegible]

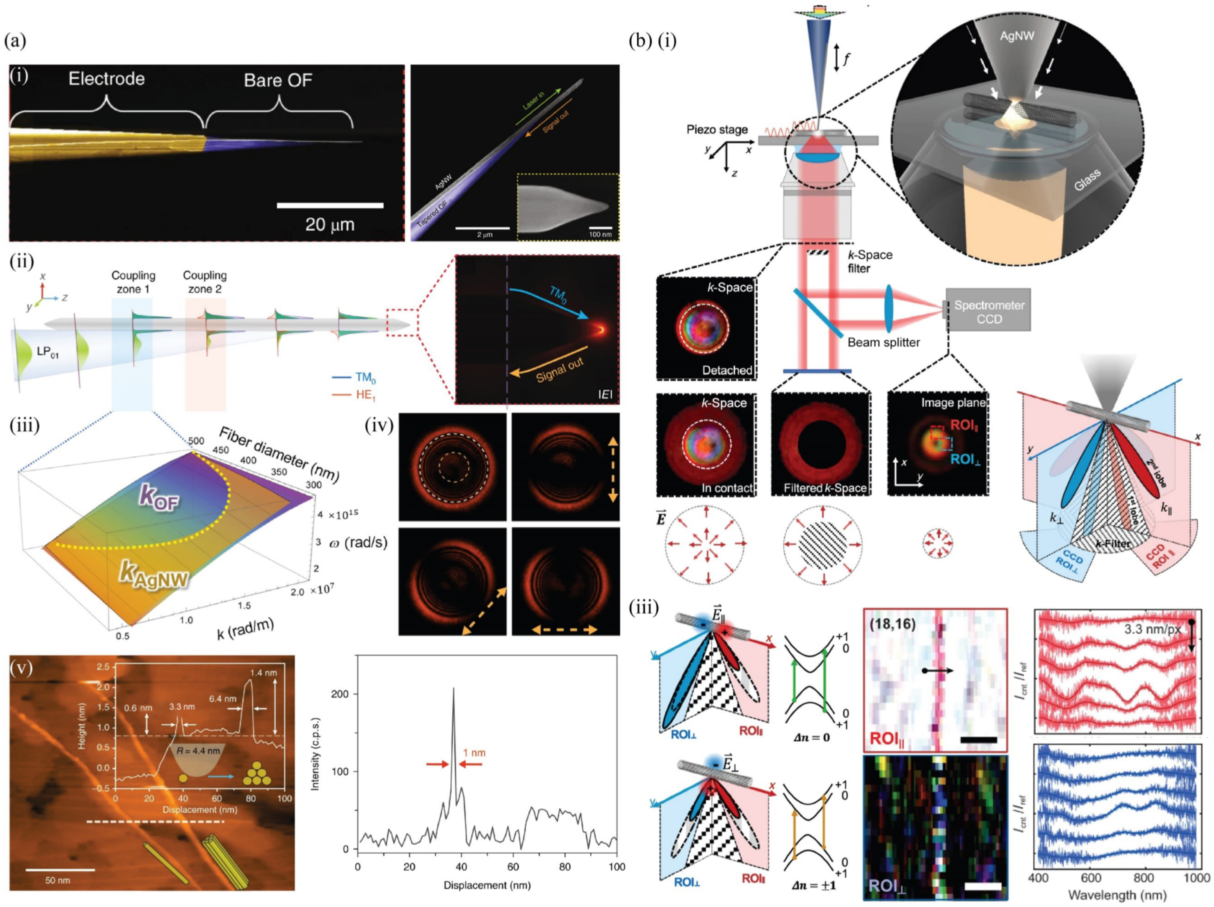

Figure 9 Nanowire-assisted selective-coupling probes. (a) The lens-free TERS ... and (iii)) schematic illustration of the LZ coupling ... the lens-free TERS mapping of a SWNT sample. Reproduced with permission from Ref. [147], © ... 2019. (b) ... schematic illustration of the imaging system. Different ROI carries di... (bottom) excitons in a SWNT show different characteristics. Reproduced with permission from Ref. [147], © Ma, X. L. / Z... et al. 2021.

milling and the skin depth ... aperture NSOM probes, the spatial resolution ... by twice the skin depth. The ... by choosing high plasmonic frequency metals, ...

4 TERS applications

Numerous successful applications of tip-enhanced Raman imaging have been demonstrated in the past decades with a ... range of research topics in materials science, surface sc... catalysis, solar cells, and so on. A remarkable breakthrough ... single-molecule TERS imaging with sub-nanometer spatial resolution. Using an STM-TERS setup integrated with a low-temperature (LT) ultrahigh-vacuum (UHV) system, Zhang et al. reported the first visualization of individual molecules by imaging their Raman response under a plasmonic gap mode [152] (Fig. 10). They also demonstrated the importance of spectral frequency matching between the nanocavity plasmon resonance and the downward molecular vibronic transitions in TERS measurement. This frequency matching can be achieved by tuning the gap distance between the probe and the sample. Recently ... et al. pushed the spatial resolution ... and directly visualized molecular ... [153]. Single-strand DNA (ssDNA) ... characterized by TERS ... sequencing of ssDNA with ... [154] in Fig. 12(a). In this experiment, ... uncoiled and deposited on ...

... including cells [155], ... [156], ... proteins [4]. ... biochemical materials have been ... TERS is also an ideal tool for ... properties of surfaces ... in electrochemical systems ... resolution. In 2019, ... of Au oxide formation at Au(111) ... spatial resolution of ... [157]. ... electrochemical potential ... sample ... ON and OFF ... was formed at defect sites under ... the OFF state, a low sample potential ... back to the metallic Au ... reversible ... site-specific ... TERS ... demonstrating the potential of ... In addition to ... Recently ... imaging has also been ... [158] ... 2017, Zhong et al. used ... spatially ... probe the site-specific ... Pd/Au(111) bimetallic ... spatial resolution ... [159] ... (TTF) ... self-assem... monolayer ...

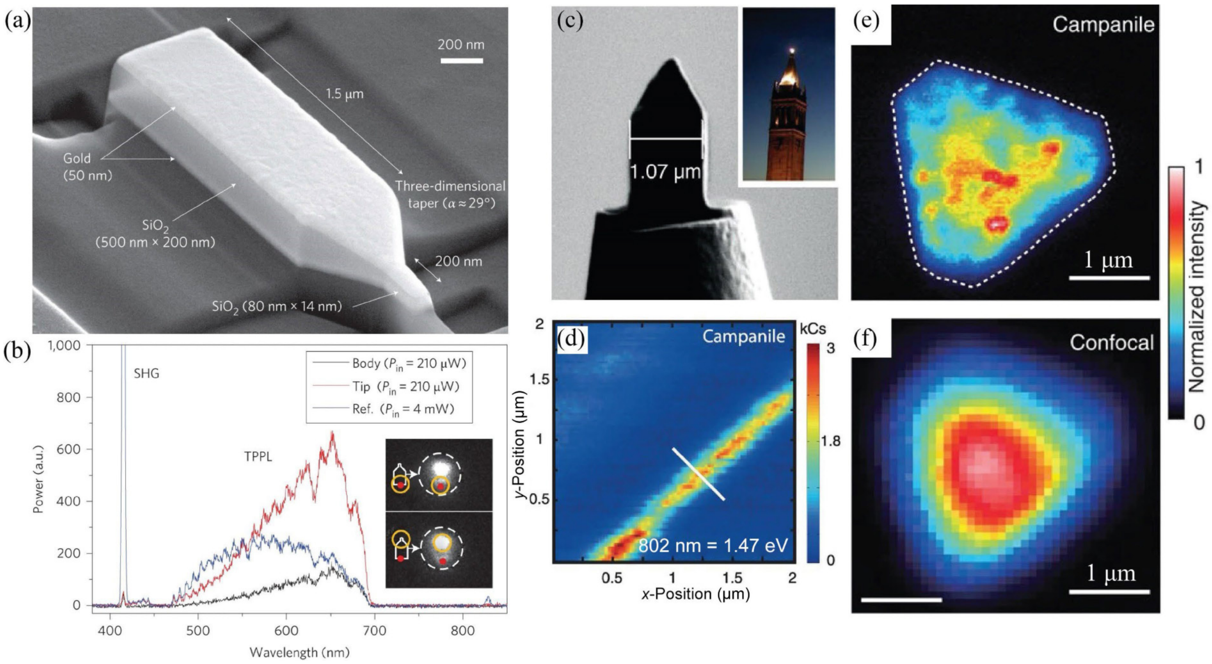

Figure 12 Tapered MIM probes. (a) The SEM image of the MIM waveguide. (b) Em[illegible] reference. Inset: two-photon photoluminescence (TPPL) images of the wave[illegible] as a red dot. (a) and (b) Reproduced with permission from Ref. [150], © Nature Publishing Group 2012. (c) The S[illegible] hyperspectral PL image of a InP nanowire mapped with [illegible] [151], © The American Association for the Advancement of Science 2012. The comparison between the campanile [illegible] PL mapping of [illegible] Reproduced with permission from Ref. [152], © [illegible] 2015.

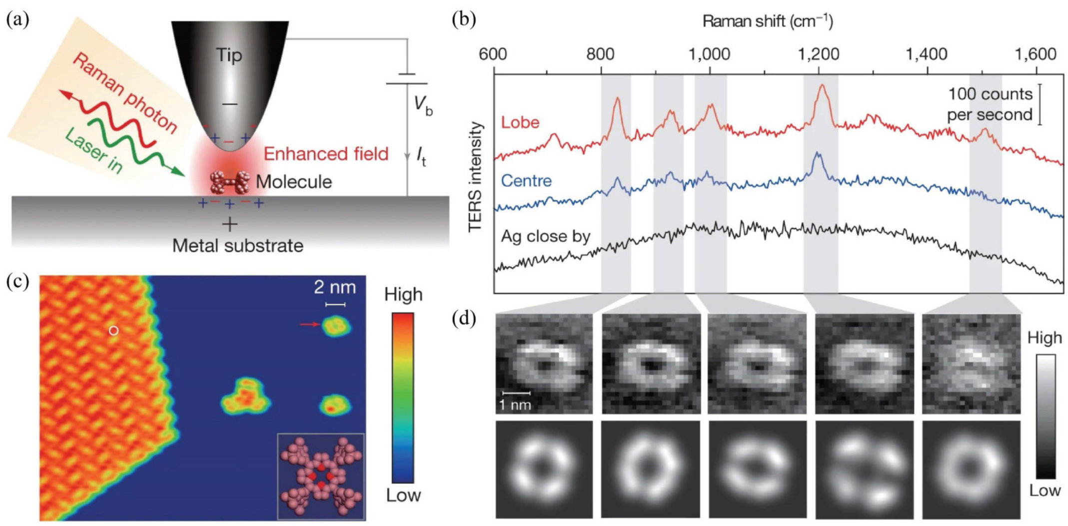

Figure 13 Single-molecule TERS imaging. (a) Schematic of the STM-based TERS [illegible] the lobe (red), center (blue), and the control spectrum of the [illegible] Reproduced with permission from Ref. [15], © Nature Publishing Group, a division of Macmillan Publis[illegible]

to metal surface atomic geometry and electronic structure [illegible] weaker at the Pd step edges than the Pd terrace. As a result, reactivity of PIC is enhanced at the Pd step edge.

Moreover, with the rapid development of 2D materials, TERS has also been utilized [161–163] to study the band structures [illegible] Huang et al. reported double Raman resonance induced by edge defects in atomically monolayer MoS_2 [illegible] identification (Fig. 13(f)) [164]. And Lee et al. investigated and identified heterogeneous defects in monolayer WS_2 [165]. In 2021, Gadelha et al. used TERS techniques to study the electronic and vibrational [illegible] graphene superlattice, revealing [illegible] phonon coupling (Fig. 13(l)) [166].

Along with developing conventional TERS probes, [illegible] nanofocusing probe designs continually present progress [illegible]

[illegible] dynamic electronic applications [illegible] demonstrated [illegible] efficiency of broadband and ultrafas[illegible] apex of grating-coupled tip [illegible] measurement, a nonlinear wave [illegible] achieved on a gold film, with [illegible] at the film edge.

5 Summary and outlook

In summary, we reviewed [illegible] focusing on the development [illegible] probes play the most essential r[illegible] of the plasmonic hotspot, the [illegible] volume [illegible]

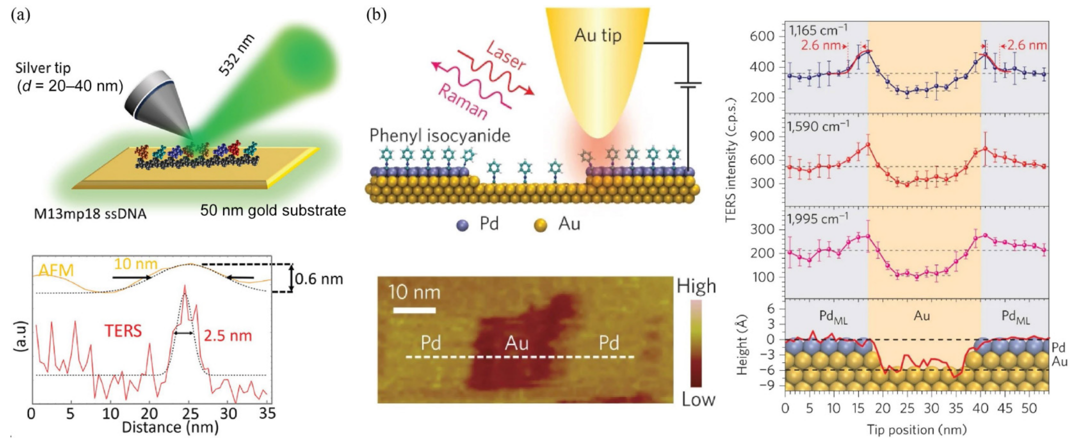

Figure 1 TERS studies for DNA molecules. (a) Contact-AFM TERS imaging of M13 [illegible] 2.5 nm is achieved. Rep[illegible] [154], © American Chemical Society 2018. (b) STM-ba[illegible] substrate. The STM image (left bottom) and TERS [illegible] [160], © Springer Nature 2016.

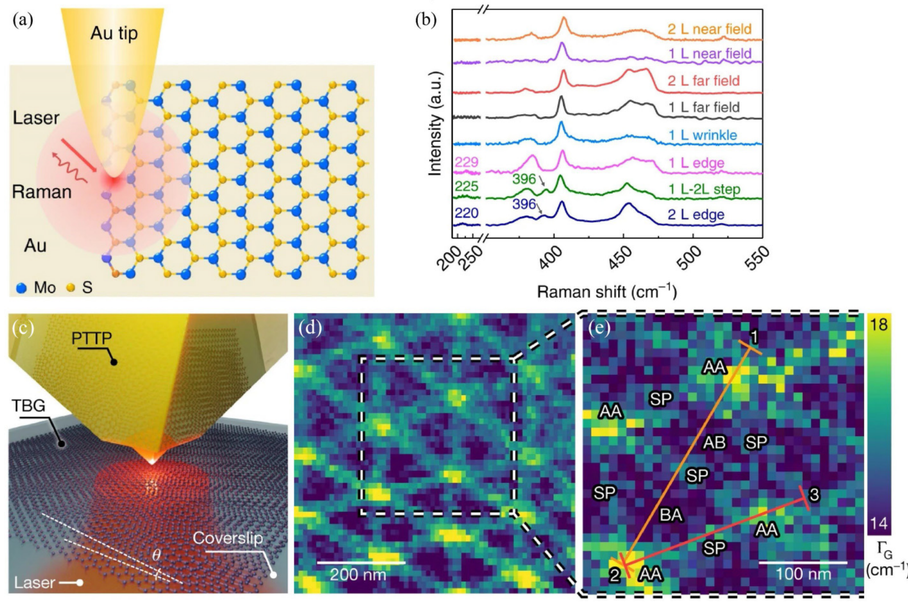

Figure 2 2D material studies enabled by TERS. (a) Schematic [illegible] Raman spectra of TERS [illegible] MoS_2 (a) and (b) Reproduced with permission from [164], © [illegible] 2019. (c) Schematics o[illegible] hyperspectral image of the twisted bilayer [illegible] (e). Reproduced with permission from [166], © [illegible] Gadelha, A. C. et al. 2021.

determines the chemical sens[illegible] the measurement. Considerable [illegible] to nov[illegible] TERS probes with a high cou[illegible] plasmonic mode for near-field [illegible] developments in probe des[illegible] Raman [illegible] nanofabrication techniques, the TERS technique has evolved into a compelling [illegible] characterization method over [illegible] chemical sensitivity of SERS [illegible] light and offering signal [illegible] correlated to the sample su[illegible] maturation of commercial TER[illegible] this technique are increasin[illegible] explored. High-performance [illegible] obstacle in the way to an [illegible] application in the surface [illegible] problem, a few critical desig[illegible]

First, most novel plasmonic [illegible] fabrication procedures, whi[illegible] prohibitive but also challen[illegible] effective, reproducible probe [illegible]

mode (TM_0). In many nanofocusing probes, remains indefinite. Since the TM_0 mode is the only one with no cut-off radius and can keep tightly bound to the metal surface throughout the nanofocusing process, maximizing the conversion efficiency from the incident light to the TM_0 mode is non-trivial in a probe design. There are two solutions for improving the TM_0 ... during the incident light-SPP coupling process: (1) using a particular structure, such as the circular Bragg gratings, asymmetric g... and photonic crystal cavity couplers. However, the TM_0 coupling efficiency can only reach less than 5% according to the rep... spatially separate the coupling regions for TM_0 and other higher order modes and let the TM_0 mode SPPs ... first. Using machine learning to optimize the coupler prof... coupling efficiency of 83% has been experimentally achieved.

It has been more than two decades since TERS was first demonstrated. Even though this period is short, numerous impressive progresses have accelerated the maturation of t... technique, and iterative commercial instrument development ... emerged. TERS has been recognized by progressively more researchers as one of the most powerful optical characteriz... tools in various fields. From our points of view, with the aforementioned problems solved in the near future, ... TERS technology can make it an important and accessible nanoscale chemical characterization tool for everyone.

Acknowledgements

This work is supported by the National Science Foundation (N... 1654746 and 1810453).

References

[1] Perry, C. H.; Hall, D. B. Temperature dependence of the raman spectrum ... $_3$. Phys. Rev. Lett. 1965, 15, 700–702.

[2] Chen, J. N.; Yang, W. S.; Dick, K.; Deppert, K.; Xu, H. Q.; Samuelson, L.; Xu, H. X. Tip-enhanced Raman scattering of p-thiocresol molecules on individual gold nanoparticles. Appl. Phys. Lett. 2008, 92, 093110.

[3] Pettinger, B.; Ren, B.; Picardi, G.; Schuster, R.; Ertl, G. Nanoscale probing of adsorbed species by tip-enhanced Raman spectroscopy. Phys. Rev. Lett. 2004, 92, 096101.

[4] Helbing, C.; Deckert-Gaudig, T.; Firkowska-Boden, I.; Wei, G.; Deckert, V.; Jandt, K. D. Protein handshake on the nanoscale: How albumin and hemoglobin self-assemble ... ACS Nano 2018, 12, 1211–1219.

[5] Dieringer, J. A.; Lettan, R. B.; Scheidt, K. A.; Van Duyne, R. P. A frequency domain existence proof ... enhanced Raman spectroscopy. J. Am. Chem. Soc. 2007, 129, 16249–16256.

[6] Fleischmann, M.; Hendra, P. J.; McQuillan, A. J. Raman spectra of pyridine adsorbed at a silver electrode. Chem. Phys. Lett. 1974, 26, 163–166.

[7] Jeanmaire, D. L.; Van Duyne, R. P. Surface Raman spectroelectrochemistry: Part I. Heterocyclic, aromatic, and aliphatic amines adsorbed on the anodized silver electrode. J. Electroanal. Chem. Interfac. Electrochem. 1977, 84, 1–20.

[8] Albrecht, M. G.; Creighton, J. A. Anomalously intense Raman spectra of pyridine at a silver electrode. J. Am. Chem. Soc. 1977, 99, 5215–5217.

[9] Nie, S. M.; Emory, S. R. Probing single molecules and single nanoparticles by surface-enhanced Raman scattering. Science 1997, 275, 1102–1106.

[10] Kneipp, K.; Wang, Y.; Kneipp, H.; Perelman, L. T.; Itzkan, I.; Dasari, R. R.; Feld, M. S. Single molecule detection using surface-enhanced raman scattering (SERS). Phys. Rev. Lett. 1997, 78, 1667–1670.

[11] Xu, W.; Li, R. H.; Wang, C. H.; ... J. Investigation of electronic ... junctions ... Nano Res. 2022, 15, 5726–5745.

[12] Cialla, D.; ... Poll..., S.; Steinbrücke... based detection ... nanoparticles ... 2014, 481 ...

[13] Ling, X.; ... Yan, R. X.; Lo, S.; H... A.; Khan, S. B.; Asiri, A. M.; Ba... Alumina-coated Ag nanocrystal mono... Raman spectroscopy platforms for ... detection of water ... Nano Lett. 2014, ... 7, 1342–1423.

[14] Born, M.; Wolf, E. Principles of Optics ... Born, M.; Wolf, ... Pergamon, 1980; pp 459 ...

[15] ... H.; Dlott, D. ... enhancements ... scattering. Science 2008, 321, 388–392.

[16] Wessel, J. Surface-enhanced optical ... Am. ... 1985, 2, 1538–1541.

[17] Stöckle, R. M.; Suh, Y. D.; Decke... chemical analysis by tip-enhanced ... Phys. Lett. 2000, 318, 131–136.

[18] Hayazawa, N.; Inouye, Y.; Sekkat, ... amplification of near-field ... Raman ... 18, 333–336.

[19] Anderson, M. S. Locally enhanced R... atomic force microscope. Appl. Phys. Lett. 2000, 76, 3130–3132.

[20] Pettinger, B.; Picardi, G.; Schuster, ... Raman spectroscopy: Towards single... Electrochemistry 2000, 68, 942–949.

[21] Steidtner, J.; Pettinger, B. Tip-e... microscopy on single dye molecules ... Phys. Rev. Lett. 2008, 100, 236101.

[22] Kurouski, D.; Zaleski, S.; Casadio, ... C. Tip-enhanced Raman spectroscop... identification of indigo and ... J. Am. Chem. Soc. 2014, 136, 8677–8684.

[23] Ichimura, T.; Hayazawa, N.; Hashim... S. Application of tip-enhanced mic... spectroscopy ... Appl. Phys. Lett. 2004, 84, 1768–1770.

[24] Urbieta, M.; Barbry, M.; Zhang, Y.; ... Zabala, N.; Aizpurua, J. Atomic-s... plasmonic picocavities: A classical ... ACS Nano 2018, 12, 585–595.

[25] Wei, H.; Xu, H. X. Hot spots in di... plasmon-enhanced Raman spectroscop... Nanoscale 2013, 5, 10794–10805.

[26] Kruger, ... Sánchez, E. J.; Xie, ... probes with optimized field enhancem... domain electromagnetic simulation. J. Chem. Phys. 2016, 120, 10895–10901.

[27] Kang, ... Jin, H. ... Kim, ... D. S.; Park, Q. ... plasmonic ... Phys. Rev. Lett. 2009, 102, 093906.

[28] McQuillan, A. J. Raman ... Furusawa, ... Hayazawa, ... Raman spectroscopy ... tip ... J. Raman Spectrosc. 2009, 40, 1324–1330.

[29] Ploi..., M.; Hayazawa, N.; Catala... A.; Hiroaki, T.; ... Tip-enhanced ... THz R... temperature ... Angew. ... Chem. 2015, 2053 ...

[30] Auttenroth, ... Fleischer, ... Exploita... Adv. ... 2014, ... 1–6 ...

[31] Anger, P.; Bharadwaj, P.; Novotny, ... of single-molecule ... Phys. Rev. Lett. 2006, 96, 113002.

[32] Buraman, ... Vainio, ... Oosten, D.; Kampf... Heideman, R.; Leinse, A.; Kuipers, ... Light ... Science 2012, 335, ... 55–58 ...

[33] Lee, ... Fleischer, ... Surface ... Simultaneous measurement of nanos... optical ... Nat. ... 2018, ... 4 ...

[34] Zhang, ... Bharadwaj, P.; Novotny, L. ... electric ... single molecule ... 2005, ... 4126 ...

[35] Fleischer, M.; Weber-Bargioni, A.; ...

A. M.; Schuck, P. J.; Cabrini, S. ... field scanning optical microscopy. ACS Nano 2015, 9, 2570–2579.

[36] Neumann, L.; Van 't Oever, J. ... scanning dipole-antenna probe for ... Nano Lett. 2013, 13, 5070–5074.

[37] Vasconcelos, T. L.; Archanjo, B. S. ... Riikonen, J.; Li, C. F.; Ribeiro ... N.; Jorio, A. et al. Tuning local... scanning near-field microscopy probes. ACS Nano 2015, 9, 6297–6304.

[38] Oliveira, B. S.; Archanjo, B. S. ... Cançado, L. G.; Jorio, A.; Vasconcelos, T. L. ... plasmon-tunable nanoantennas for tip-enhanced Raman spectroscopy. J. Chem. Phys. 2020, 153, 114201.

[39] Tschannen, C. D.; Frimmer, M.; ... Pichler, T.; Novotny, L. Tip-enhanced ... from carbyne. Nano Lett. 2022, 22, 3260–3265.

[40] Richard-Lacroix, M.; Deckert, V. Direct molecular-level near-field plasmon and temperature assessment in a single plasmonic hotspot. Light Sci. Appl. 2020, 9, 35.

[41] Vasconcelos, T. L.; Archanjo, B. S.; Oliveira, B. S.; Silva, W. F. ... Alencar, R. S.; Rabelo, C.; Achete, C. A.; Jorio, A.; Cançado, L. G. Optical nanoantennas for tip-enhanced Raman spectroscopy. IEEE J. Sel. Top. Quantum Electron. 2021, 27, 4600411.

[42] Zhang, Z. L.; Sheng, S. X.; Wang, R. M.; Sun, M. T. Tip-enhanced raman spectroscopy. Anal. Chem. 2016, 88, 9328–9346.

[43] Stadler, J.; Schmid, T.; Zenobi, R. Developments in and practical guidelines for tip-enhanced Raman spectroscopy. Nanoscale 2012, 4, 1856–1870.

[44] Kumar, N.; Rae, A.; Roy, D. Accurate measurement of enhancement factor in tip-enhanced Raman spectroscopy through elimination of far-field artefacts. Appl. Phys. Lett. 2014, 104, 123106.

[45] Kravtsov, V.; Ulbricht, R.; Atkin, J. M.; Raschke, M. B. Plasmonic nanofocused four-wave mixing for femtosecond near-field imaging. Nat. Nanotechnol. 2016, 11, 459–464.

[46] Pile, D. F. P.; Gramotnev, D. K. Adiabatic and nonadiabatic nanofocusing of plasmons by tapered gap plasmon waveguides. Appl. Phys. Lett. 2006, 89, 041111.

[47] Vernon, K. C.; Gramotnev, D. K.; Pile, D. F. Adiabatic nanofocusing of plasmons by a sharp metal wedge on a dielectric substrate. J. Appl. Phys. 2007, 101, 104312.

[48] Stockman, M. I. Nanofocusing of optical energy in tapered plasmonic waveguides. Phys. Rev. Lett. 2004, 93, 137404.

[49] Giugni, A.; Torre, B.; Toma, A.; Francardi, M.; Malerba, M.; Alabastri, A.; Zaccaria, R. P.; Stockman, M. I.; Di Fabrizio, E. Hot-electron nanoscopy using adiabatic compression of surface plasmons. Nat. Nanotechnol. 2013, 8, 845–852.

[50] Nerkararyan, K. V. Superfocusing of a surface polariton in a wedge-like structure. Phys. Lett. A 1997, 237, 103–105.

[51] Dakss, M. L.; Kuhn, L.; Heidrich, P. F.; Scott, B. A. Grating coupler for efficient excitation of optical guided waves in thin films. Appl. Phys. Lett. 1970, 16, 523–525.

[52] De Angelis, F.; Das, G.; Candeloro, P.; Patrini, M.; Galli, M.; Bek, A.; Lazzarino, M.; Maksymov, I.; Liberale, C.; Andreani, L. C. et al. Nanoscale chemical mapping using three-dimensional adiabatic compression of surface plasmon polaritons. Nat. Nanotechnol. 2010, 5, 67–72.

[53] Janunts, N. A.; Baghdasaryan, K. S.; Nerkararyan, K. V.; Hecht, B. Excitation and superfocusing of surface plasmon polaritons on a silver-coated optical fiber tip. Opt. Commun. 2005, 253, 118–124.

[54] Kim, S.; Yu, N.; Ma, X. Z.; Zhu, Y. Z.; Liu, Q.; Liu, M.; Yan, R. X. High external-efficiency nanofocusing for lens-free near-field optical nanoscopy. Nat. Photonics 2019, 13, 636–643.

[55] Wei, H.; Xu, H. Nanowire-based plasmonic waveguides and devices for integrated nanophotonic circuits. Nanophotonics 2012, 1, 155–169.

[56] Bao, W.; Borys, N. J.; Ko, C.; Suh, J.; Fan, W.; Thron, A.; Zhang, Y. J.; Buyanin, A.; Zhang, J.; Cabrini, S. et al. Visualizing nanoscale excitonic relaxation properties of disordered edges and grain boundaries in monolayer molybdenum disulfide. Nat. Commun. 2015, 6, 7993.

[57] Richard-Lacroix, M.; Zhang, Y.; Dong, Z. C.; Deckert, V. Mastering high resolution tip-enhanced Raman spectroscopy: Towards a shift of perception. Chem. Soc. Rev. 2017, 46, 3922–3944.

[58] Fragneaud, B.; Oliveira, B. S. ... Yu, D. J. S.; Rabelo, C.; Rodrigues, T.; Wa... ... tip-enhanced Raman ... 2021, 12, 123110.

[59] Yeo, B. S.; Zhang, W.; Vannier, C.; Zenobi, R. ... Raman signals with ... Appl. Spectrosc. 2006, 60, 1142–1147.

[60] Zhang, M.; Wang, J. ... Plasmonic lens ... excitation for tip-enhanced Raman ... Nanoscale Res. Lett. 2015, 10, 189.

[61] Hayazawa, N.; Saito, Y.; Kawata, S. ... stokes-anti-stokes scattering of longitudinal field for tip-enhanced ... Appl. Phys. Lett. 2004, 85, 6239–6241.

[62] Lieb, M. A.; Meixner, A. J. A high ... mirror as imaging device for ... Opt. Express 2001, 8, 458–474.

[63] Zhang, D.; Wang, X.; Braun, K.; Egelhaaf, H. J.; Fleischer, M.; Hennemann, L.; Hintz, H.; Stanciu, C. ... et al. Parabolic mirror-assisted tip-enhanced Raman spectroscopy for non-transparent samples. J. Raman Spectrosc. 2009, 40, 1371–1376.

[64] Kazemi-Zanjani, N.; Vedraine, S.; L... ... enhancement of electric field in t... using radially and linearly polari... Opt. Express 2013, 21, 25271–25276.

[65] Fan, Y.; Jin, D.; Wu, X. J.; Fang ... hotspot alignment in tip-enhanced ... silver photoluminescence ... Sensors 2020, 20, 6687.

[66] Wang, H. F.; Shi, L. P.; Lukyanchuk, B.; ... T. Creation of a needle of longitudinal ... using binary optics. Nat. Photonics 2008, 2, 501–505.

[67] Zhan, Q. W. Evanescent Bessel beam ... plasmon resonance excitation by a ... Opt. Lett. 2006, 31, 1726–1728.

[68] Jia, H. W.; Liu, H. T.; Zhong, Y. ... polaritons and other waves in the ... dipole ... Sci. Rep. 2015, 5, 8456.

[69] Meng, L. Y.; Yang, Z. L. Directional ... emission of tilted-tip enhanced ... Nanophotonics 2018, 7, 1325–1332.

[70] Sifat, A. A.; Potma, E. O. Optimiz... properties of tips in tip-enhanced ... J. Raman Spectrosc. 2021, 52, 2208–2208.

[71] Stadler, J.; Schmid, T.; Zenobi, R. ... using top-illumination tip-enhanced ... Nano Lett. 2010, 10, 4514–4520.

[72] Issa, N. A.; Guckenberger, R. Fluo... roles of energy transfer and surf... Opt. Express 2007, 15, 12131–12144.

[73] Yang, Z. L.; Li, Q. H.; Ruan, F. X. ... radiative decay and nonradiative ... Chem. Phys. Lett. 2004, 396, 2–7.

[74] Müller, A. D.; Müller, F.; Hietschold ... Dickmann, K. Characterization of ... tungsten tips for scanning tunneling ... 1999, 79, 3–9.

[75] Neacsu, C. C.; Steudle, G. A.; Raschke ... scattering from ... Appl. Phys. B 2005, 80, 295–300.

[76] Eligal, L.; Culfaz, F.; McCaughan, ... Etching gold tips suitable for tip-enhanced ... microscopy. Rev. Sci. Instrum. 2009, 80, 033701.

[77] Schambach, P. Tip-enhanced Raman s... vacuum. Ph.D. Dissertation, Friedrich ... 2013.

[78] Kharintsev, S. S.; Rogov, A. M.; Kazarian, S. G. Nanoscale imaging and tuning of optical taper antenna for tip-enhanced Raman scattering. Rev. Sci. Instrum. 2013, 84, 093106.

[79] Ren, B.; Picardi, G.; Pettinger, B. Preparation of gold tips suitable for tip-enhanced Raman spectroscopy and light emission by electrochemical etching. Rev. Sci. Instrum. 2004, 75, 837–841.

[80] Wang, X.; Liu, Z.; Zhuang, M. D.; Zhang, H. M.; Wang, X.; Xie, Z. X.; Wu, D. Y.; Ren, B.; Tian, Z. Q. Tip-enhanced Raman spectroscopy for investigating adsorbed species on a single-crystal surface using electrochemically prepared Au tips. Appl. Phys. Lett. 2007, 91, 101105.

[81] Liu, Q. S.; Kim, S.; Ma, X. Z.; Yu, N.; Zhu, Y. L.; Deng, S. H.; Yan, R. X.; Zhao, H. J.; Liu, M. Ultra-sharp and surfactant-free silver nanowire for scanning tip-enhanced Raman spectroscopy. Nanoscale 2019, 11, 7790–7797.

[82] Bailo, E.; Deckert, V. Tip-enhanced Raman spectroscopy of single RNA strands: Towards a novel direct-sequencing method. Angew. Chem., Int. Ed. 2008, 47, 1658–1661.

[83] Mino, T.; Saito, Y.; Verma, P. Quantitative analysis of polarization-controlled tip-enhanced Raman imaging through the evaluation of the tip dipole. ACS Nano 2014, 8, 10187–10195.

[84] Chen, H. K.; Zhang, Y. Q.; Dai, Y. C.; Min, C. J.; Zhu, S. W.; Yuan, X. C. Facilitated tip-enhanced Raman scattering by focused gap-plasmon hybridization. Photonics Res. 2020, 8, 103–109.

[85] Capaccio, A.; Sasso, A.; Tarallo, O.; Rusciano, G. Coupled plasmonic probes for tip-enhanced Raman spectroscopy. Nanoscale 2020, 12, 24376–24384.

[86] Taguchi, A.; Yu, J.; Verma, P.; Kawata, S. Optical antennas with multiple plasmonic nanoparticles for tip-enhanced Raman microscopy. Nanoscale 2015, 7, 17424–17433.

[87] Mahmoodi, N.; Rushdi, A. I.; Bowen, J.; Sabouri, A.; Anthony, C. J.; Mendes, P. M.; Preece, J. A. Room temperature thermally evaporated thin Au film on Si suitable for application of thiol self-assembled monolayers in micro/nano-electro-mechanical-systems sensors. J. Vac. Sci. Technol. A 2017, 35, 041514.

[88] Johnson, T. W.; Lapin, Z. J.; Beams, R.; Lindquist, N. C.; Rodrigo, S. G.; Novotny, L.; Oh, S. H. Highly reproducible near-field optical imaging with sub-20-nm resolution based on template-stripped gold pyramids. ACS Nano 2012, 6, 9168–9174.

[89] Vasconcelos, T. L.; Archanjo, B. S.; Oliveira, B. S.; Valaski, R.; Cordeiro, R. C.; Medeiros, H. G.; Rabelo, C.; Ribeiro, A.; Ercius, P.; Achete, C. A. et al. Plasmon-tunable tip pyramids: Monopole nanoantennas for near-field scanning optical microscopy. Adv. Opt. Mater. 2018, 6, 1800528.

[90] Höppener, C.; Lapin, Z. J.; Bharadwaj, P.; Novotny, L. Self-similar gold-nanoparticle antennas for a cascaded enhancement of the optical field. Phys. Rev. Lett. 2012, 109, 017402.

[91] Leiterer, C.; Deckert-Gaudig, T.; Singh, P.; Wirth, J.; Deckert, V.; Fritzsche, W. Dielectrophoretic positioning of single nanoparticles on atomic force microscope tips for tip-enhanced Raman spectroscopy. Electrophoresis 2015, 36, 1142–1148.

[92] Ma, X.; Grüßer, M.; Schuster, R. [illegible] hand-Local electrochemical deposition of [illegible] of optically inactive [illegible] tips. Appl. Phys. Lett. [illegible] 241103.

[93] Dill, T. J.; Rozin, M. J.; Palani, S.; Tao, A. R. Colloidal nanoantennas for hyperspectral chemical mapping. ACS Nano 2016, 10, 7523–7531.

[94] Walke, P.; Toyouchi, S.; Wolf, M.; Inose, T.; De Feyter, S.; Fujita, Y.; Uji-i, H. Tip-enhanced Raman scattering on dielectric substrates via electrical cutting of silver nanowire. J. Phys. Chem. Lett. 2018, 9, 7117–7122.

[95] Farahani, J. N.; Eisler, H. J.; Pohl, D. W.; Pavius, M.; Flückiger, P.; Gasser, P.; Hecht, B. Bow-tie optical antenna probes for single-emitter scanning near-field optical microscopy. Nanotechnology 2007, 18, 125506.

[96] Guo, R.; Kinzel, E. C.; Li, Y.; Uppuluri, S. M.; Raman, A.; Xu, X. F. Three-dimensional mapping of optical near field of a nanoscale bowtie antenna. Opt. Express 2010, 18, 4961–4971.

[97] Farahani, J. N.; Pohl, D. W.; Eisler, H. J.; Hecht, B. Single quantum dot coupled to a scanning optical antenna: A tunable superemitter. Phys. Rev. Lett. 2005, 95, 017402.

[98] [illegible] tomography and local electric-field [illegible] plasmonic [illegible]. ACS Photonics 2015, 2, 428–438.

[99] Lindquist, N. C.; Jose, J.; Cherukulappurath, S.; Chen, X. S.; Johnson, T. W.; Oh, S. H. Tip-based plasmonics: Squeezing light with metallic nanoprobes. Laser Photonics Rev. 2013, 7, 453–477.

[100] Wang, Y.; Srituravanich, W.; Sun, C.; Zhang, X. Plasmonic nearfield scanning probe with high transmission. Nano Lett. 2008, 8, 3041–3045.

[101] Taminiau, T. H.; Moerland, R. J.; Segerink, F. B.; Kuipers, L.; van Hulst, N. F. λ/4 Resonance of an optical monopole antenna probed by single molecule fluorescence. Nano Lett. 2007, 7, 28–33.

[102] van Zanten, T. S.; Lopez-Bosque, M. J.; Garcia-Parajo, M. F. Imaging individual proteins and nanodomains on intact cell membranes with a probe-based optical antenna. Small 2010, 6, 270–275.

[103] Husnik, M.; Klein, M. W.; Feth, N.; König, M.; Niegemann, J.; Busch, K.; Linden, S.; Wegener, M. Absolute extinction cross-section of individual magnetic split-ring resonators. Nat. Photonics 2008, 2, 614–617.

[104] Babadjanyan, A. J.; Margaryan, N. L.; Nerkararyan, K. V. Superfocusing of surface polaritons in the conical structure. J. Appl. Phys. 2000, 87, 3785–3788.

[105] [illegible] Optical mode evolution [illegible] coupled surface plasmon [illegible]. Opto-Electron. Adv. 2018, 1, 180010.

[106] Kim, S.; [illegible] surface plasmon polariton (SPP) mode [illegible] waveguide [illegible].

[107] Issa, N. A.; Guckenberger, R. Optical nanofocusing on tapered metallic waveguides. Plasmonics 2007, 2, 31–37.

[108] [illegible] Appl. [illegible] 034311.

[109] Neacsu, C. C.; Berweger, S.; Olmon, R. L.; Saraf, L. V.; Ropers, C.; Raschke, M. B. Near-field localization in plasmonic superfocusing: A nanoemitter on a tip. Nano Lett. 2010, 10, 592–596.

[110] [illegible] J. T.; Xie, [illegible].

[111] Ropers, C.; Neacsu, C. C.; Elsaesser, T.; Albrecht, M.; Raschke, M. B.; Lienau, C. Grating-coupling of surface plasmons onto metallic tips: A nanoconfined light source. Nano Lett. 2007, 7, 2784–2788.

[112] Fang, Y.; Wei, H.; Hao, F.; Nordlander, P.; Xu, H. X. Remote-excitation surface-enhanced Raman scattering using propagating Ag nanowire plasmons. Nano Lett. 2009, 9, 2049–2053.

[113] [illegible] Interfacing photonic crystal fiber [illegible] enhanced light [illegible].

[114] [illegible] M.; Kambayashi, T.; Okamoto, T.; Kobayashi, K. et al. Low-background tip-enhanced Raman spectroscopy enabled by a plasmon [illegible]. Anal. Chem. 2019, 91, [illegible].

[115] Berweger, S.; Atkin, J. M.; Olmon, R. L.; Raschke, M. B. Adiabatic tip-plasmon focusing for nano-Raman spectroscopy. J. Phys. Chem. Lett. 2010, 1, 3427–3432.

[116] [illegible] C.; Sun, J. H.; Xiao, X.; Sun, [illegible]; Yu, J. Z.; Yu, Y. D. High efficiency [illegible] nanometallic probes for single-[illegible].

[117] Umakoshi, T.; Saito, Y.; Verma, P. Highly efficient plasmonic tip design for plasmon nanofocusing in near-field optical microscopy. Nanoscale 2016, 8, 5634–5640.

[118] Umakoshi, T.; Tanaka, M.; Saito, Y.; Verma, P. White nanolight source for optical nanoimaging. Sci. Adv. 2020, 6, eaba4179.

[119] Esmann, M.; Becker, S. F.; Da Cunha, B. B.; Brauer, J. H.; Vogelgesang, R.; Groß, P.; Lienau, C. k-space imaging of the eigenmodes of sharp gold tapers for scanning near-field optical microscopy. Beilstein J. Nanotechnol. 2013, 4, 603–610.
[120] Knight, M. W.; Grady, N. K.; Bardhan, R.; Hao, F.; Nordlander, P.; Halas, N. J. Nanoparticle-mediated coupling of light into a nanowire. Nano Lett. 2007, 7, 2346–2350.
[121] Lu, G.; De Keersmaecker, H.; Su, L.; Kenens, B.; Rocha, S.; Fron, E.; Chen, C.; Van Dorpe, P.; Mizuno, H.; Hofkens, J. et al. Live-cell SERS endoscopy using plasmonic nanowire waveguides. Adv. Mater. 2014, 26, 5124–5128.
[122] Ma, X. Z.; Zhu, Y. Z.; Yu, N.; Kim, S.; Liu, Q. S.; Apontti, L.; Xu, D.; Yan, R. X.; Liu, M. Towards high-contrast atomic force microscopy-tip-enhanced Raman spectroscopy imaging: Nanoantenna-mediated remote-excitation on sharp-tip silver nanowire probes. Nano Lett. 2019, 19, 100–107.
[123] Jiang, R. H.; Chen, C.; Lin, D. Z.; Chou, H. C.; Chu, J. Y.; Yen, T. J. Near-field plasmonic probe with super resolution and high throughput and signal-to-noise ratio. Nano Lett. 2018, 18, 881–885.
[124] Li, S. B.; Yang, S. M.; Wang, [illegible] Rosenwaks, Y. Plasmonic interference modulation for broadband nanofocusing. Nanophotonics 2021, 10, 4113–4123.
[125] Stegeman, G. I.; Wallis, R. F.; Maradudin, A. A. Excitation of surface polaritons by end-fire coupling. Opt. Lett. 1983, 8, 386–388.
[126] Fisher, C.; Botten, L. C.; Poulton, C. G.; McPhedran, R. C.; De Sterke, C. M. End-fire coupling efficiencies of surface plasmons for silver, gold, and plasmonic nitride compounds. J. Opt. Soc. Am. B 2016, 33, 1044–1054.
[127] Fisher, C.; Botten, L. C.; Poulton, C. G.; McPhedran, R. C.; De Sterke, C. M. Efficient end-fire coupling of surface plasmons on flat metal waveguides. J. Opt. Soc. Am. B 2015, 32, 412–425.
[128] Masuda, H.; Fukuda, K. Ordered metal nanohole arrays made by a two-step replication of honeycomb structures of anodic alumina. Science 1995, 268, 1466–1468.
[129] Yao, J.; Liu, Z. W.; Liu, Y. M.; Wang, Y.; Sun, C.; Bartal, G.; Stacy, A. M.; Zhang, X. Optical negative refraction in bulk metamaterials of nanowires. Science 2008, 321, 930.
[130] Sun, Y. G.; Yin, Y. D.; Mayers, B. T.; Herricks, T.; Xia, Y. N. Uniform silver nanowires synthesis by reducing $AgNO_3$ with ethylene glycol in the presence of seeds and poly(vinyl pyrrolidone). Chem. Mater. 2002, 14, 4736–4745.
[131] Ditlbacher, H.; Hohenau, A.; Wagner, D.; Kreibig, U.; Rogers, M.; Hofer, F.; Aussenegg, F. R.; Krenn, J. R. Silver nanowires as surface plasmon resonators. Phys. Rev. Lett. 2005, 95, 257403.
[132] Sanders, A. W.; Routenberg, D. A.; Wiley, B. J.; Xia, Y. N.; Dufresne, E. R.; Reed, M. A. Observation of plasmon propagation, redirection, and fan-out in silver nanowires. Nano Lett. 2006, 6, 1822–1826.
[133] Pyayt, A. L.; Wiley, B.; Xia, Y. N.; Chen, A.; Dalton, L. Integration of photonic and silver nanowire plasmonic waveguides. Nat. Nanotechnol. 2008, 3, 660–665.
[134] Yan, R. X.; Park, J. H.; Choi, Y.; Heo, C. J.; Yang, S. M.; Lee, L. P.; Yang, P. D. Nanowire-based single-cell endoscopy. Nat. Nanotechnol. 2012, 7, 191–196.
[135] Yan, R. X.; Pausauskie, P.; Huang, J. X.; Yang, P. D. Direct photonic–plasmonic coupling and routing in single nanowires. Proc. Natl. Acad. Sci. USA 2009, 106, 21045–21050.
[136] Guo, X.; Qiu, M.; Bao, J. M.; Wiley, B. J.; Yang, Q.; Zhang, X. N.; Ma, Y. G.; Yu, H. K.; Tong, L. M. Direct coupling of plasmonic and photonic nanowires for hybrid nanophotonic components and circuits. Nano Lett. 2009, 9, 4515–4519.
[137] Lee, H. W.; Schmidt, M. A.; Russell, R. F.; Joly, N. Y.; Tyagi, H. K.; Uebel, P.; Russell, P. S. J. Pressure-assisted melt-filling and optical characterization of Au nano-wires in microstructured fibers. Opt. Express 2011, 19, 12180–12189.
[138] Chen, X. W.; Sandoghdar, V.; Agio, M. Highly efficient interfacing of guided plasmons and photons in nanowires. Nano Lett. 2009, 9, 3756–3761.
[139] Tuniz, A.; Chemnitz, M.; Dellith, J.; Weidlich, S.; Schmidt, M. A. Hybrid-mode-assisted long-distance excitation of short-range surface plasmons in a nanotip-enhanced step-index fiber. Nano Lett. 2017, 17, 631–637.
[140] Khomeriki, R.; Ruffo, S. Nonadiabatic Landau-Zener tunneling in waveguide arrays with a step in the refractive index. Phys. Rev. Lett. 2005, 94, 113904.
[141] Bouhelier, A.; Renger, J.; Beversluis, M. R.; Novotny, L. Plasmon-coupled tip-enhanced near-field optical microscopy. J. Microsc. 2003, 210, 220–224.
[142] [illegible] Janunts, N.; Klein, [illegible] Diziain, S.; Sison, M.; Kley, E. B. [illegible] Plasmonic [illegible] based [illegible] excitation [illegible] ACS Photonics 2015, 2, 1468–1475.
[143] Ding, W.; Andrews, S. R.; Maier, S. A. Internal excitation and superfocusing of surface plasmon polaritons on a silver-coated optical fiber tip. Phys. Rev. A 2007, 75, 063822.
[144] [illegible] Jiang, L. Y.; Chen, H. Y.; Zhao, [illegible] Asymmetric [illegible] nanoprobe for plasmonic [illegible] broadband [illegible] ACS Photonics 2018, 5, [illegible].
[145] Mrejen, M.; Suchowski, H.; Hatakeyama, T.; Wu, C. H.; Feng, L.; O'Brien, K.; Wang, Y.; Zhang, X. Adiabatic elimination-based coupling control in densely packed subwavelength waveguides. Nat. Commun. 2015, 6, 7565.
[146] [illegible] McPhedran, R. C. [illegible] Efficiencies of surface plasmon [illegible] design of a photonic-plasmonic superfocusing interface. ACS Appl. Mater. Interfaces 2022, 14, [illegible].
[147] Ma, X. Z.; Liu, Q. S.; Yu, N.; Xu, D.; Kim, S.; Liu, Z. Y.; Jiang, K. L.; Wong, B. M.; Yan, R. X.; Liu, M. 6 nm super-resolution optical transmission and scattering spectroscopic imaging of carbon nanotubes using a nanometer-scale white light source. Nat. Commun. 2021, 12, 6868.
[148] Choi, H.; Pile, D. F. P.; Nam, S.; Bartal, G.; Zhang, X. Compressing surface plasmons for nano-scale optical focusing. Opt. Express 2009, 17, 7519–7524.
[149] Gramotnev, D. K. [illegible] nanofocusing [illegible] Appl. Phys. 2005, 98, 104302.
[150] Choo, H.; Kim, M. K.; Staffaroni, M.; Seok, T. J.; Bokor, J.; Cabrini, S.; Schuck, P. J.; Wu, M. C.; Yablonovitch, E. Nanofocusing in a metal–insulator–metal gap plasmon waveguide with a three-dimensional linear taper. Nat. Photonics 2012, 6, 838–844.
[151] Bao, W.; Melli, M.; Caselli, N.; Riboli, F.; Wiersma, D. S.; Staffaroni, M.; Choo, H.; Ogletree, D. F.; Aloni, S.; Bokor, J. et al. Mapping local charge recombination heterogeneity by multidimensional nanospectroscopic imaging. Science 2012, 338, 1317–1321.
[152] Zhang, R.; Zhang, Y.; Dong, Z. C.; Jiang, S.; Zhang, C.; Chen, L. G.; Zhang, L.; Liao, Y.; Aizpurua, J.; Luo, Y. et al. Chemical mapping of a single molecule by plasmon-enhanced Raman scattering. Nature 2013, 498, 82–86.
[153] Lee, J.; Crampton, K. T.; Tallarida, N.; Apkarian, V. A. Visualizing vibrational normal modes of a single molecule with atomically confined light. Nature 2019, 568, 78–82.
[154] He, Z.; Han, Z. H.; Kizer, M.; Linhardt, R. J.; Wang, X.; Sinyukov, A. M.; Wang, J. Z.; Deckert, V.; Sokolov, A. V.; Hu, J. et al. Tip-enhanced Raman imaging of single-stranded DNA with single base resolution. J. Am. Chem. Soc. 2019, 141, 753–757.
[155] Neugebauer, U.; Schmid, U.; Baumann, K.; Ziebuhr, W.; Kozitskaya, S.; Deckert, V.; Schmitt, M.; Popp, J. Towards a detailed understanding of bacterial metabolism—Spectroscopic characterization of Staphylococcus epidermidis. ChemPhysChem 2007, 8, 124–137.
[156] Paulite, M.; Blum, C.; Schmid, T.; Opilik, L.; Eyer, K.; Walker, G. C.; Zenobi, R. Full spectroscopic tip-enhanced Raman imaging of single nanotapes formed from β-amyloid(1–40) peptide fragments. ACS Nano 2013, 7, 911–920.

[157] Pfisterer, J. H. K.; Baghernejad, M.; [illegible] Reactivity mapping of nanoscale [illegible] electrochemical [illegible] Nat. Commun. 2019, 10, 5702.

[158] Piergies, N.; Pięta, E.; Paluszkiewicz, C.; [illegible] M. Polarization effect in tip-en[illegible] studies of the selective Y5 [illegible] Nano Res. 2018, 11, 4401–4411.

[159] Li, X. P.; Liang, Z. S.; Zhang, [illegible] micrometer-scale chemical analys[illegible] tip-enhanced ablation and ion[illegible] spectr[illegible] Nano Res. 2018, 11, 5989–5996.

[160] Zhong, J. H.; Jin, X.; Meng, L. [illegible] L.; Williams, C. T.; Ren, B. Pr[illegible] properties of a bimetalli[illegible] nanote[illegible] 2017, 12, 132–136.

[161] Carozo, V.; Almeida, C. M.; F[illegible] Achete, C. A.; Jorio, A. Raman s[illegible] Nano Lett. 2011, 11, 4527–4534.

[162] Smolsky, J. M.; Krasnoslobodtsev, A. V. [illegible]

[illegible] Nano Lett. 2018, 18, 6839–[illegible]

[163] Alencar, R. S.; Rabelo, C.; Miranda[illegible] Oliveira, B. S.; [illegible] enhanced raman [illegible] Nano Lett. 2019, 19, 7357–7364.

[164] [illegible] Commun. 2019, 10, 5544.

[165] [illegible] Raman spectrosc[illegible] 2012, [illegible]

[166] [illegible] Vasconcelos, [illegible] Miranda, D.; Nadas, R. et al. Loca[illegible] Nano Lett. 2019, 19, [illegible]